RSC Advances

PAPER

View Article Online
View Journal | View Issue

Cite this: *RSC Adv.*, 2017, **7**, 13281

Broad red-emission of $Sr_3Y_2Ge_3O_{12}:Eu^{2+}$ garnet phosphors under blue excitation for warm WLED applications

Sk. Khaja Hussain and Jae Su Yu*

Eu^{2+} ions activated $Sr_3Y_2Ge_3O_{12}$ (SYGO) phosphors were synthesized by an efficient pechini-type sol–gel method. X-ray diffractometry, Fourier transform infrared spectrometry, field-emission transmission electron microscopy, and spectrofluorometry measurements were performed to characterize the prepared phosphor samples after annealing under thermal CO reducing atmosphere. The phosphors showed nearly spherical-shaped morphology and their phase was identified to be cubic with the space group $la\bar{3}d$ (230). Under 468 nm blue excitation, the SYGO:Eu^{2+} phosphors exhibited a broadband red emission at 612 nm due to the $4f^6 5d^1 \rightarrow 4f^7$ electronic transition of Eu^{2+} ions. Temperature-dependent photoluminescence (PL) emission properties, PL decay profile and quantum yield were measured for the optimized SYGO:0.01 mol Eu^{2+} (SYGO:0.01Eu^{2+}) red phosphor. Furthermore, a white light-emitting diode (WLED) device was also fabricated by blending the SYGO:0.01Eu^{2+} red phosphor with a commercially available $Y_3Al_5O_{12}:Ce^{3+}$ (YAG:Ce^{3+}) yellow phosphor on a 452 nm blue LED chip under 30 mA forward-bias current. The fabricated YAG:Ce^{3+}/SYGO:0.01Eu^{2+}-based WLED device showed Commission International de l'eclairage chromaticity coordinates in the natural white region (0.3300, 0.3439) with good color rendering index and correlated color temperature of 85.81 and 5483 K, respectively. These results imply that the SYGO:0.01Eu^{2+} is a potential red phosphor to obtain the warm white light under blue excitations.

Received 12th December 2016
Accepted 20th February 2017

DOI: 10.1039/c6ra28069b

rsc.li/rsc-advances

Introduction

In recent years, white light-emitting diodes (WLEDs) which are a so-called next-generation solid-state lighting source have been extensively employed in backlights, automobile headlights, and flashlights.[1–5] Currently, these devices are gradually replacing traditional incandescent and florescent lamps owing to their bright features of high energy efficiency, long lifetime, high durability, cost-effectiveness and environmental compatibility characteristics.[3,6–9] It is well known that commercial WLEDs are fabricated by a fairly broad spectral power distribution of a yellow-emitting Ce^{3+}-doped $Y_3Al_5O_{12}$ (YAG) phosphor dispersed in an epoxy resin and coated on a blue-emitting InGaN LED (450–470 nm) chip.[10,11] When the YAG:Ce^{3+} phosphor is combined with the blue LED chip, the part of blue light is converted into yellow light *via* the phosphor and the remaining part of light stays with the yellow light, thus resulting in a cool white light. Therefore, the commercial YAG:Ce^{3+}-based WLEDs generate only cool white light because of their lack of a red component in the spectral region, which exhibits low color-rendering index (CRI) (*i.e.*, CRI < 80) as well as high color temperature (CCT).[4,12,13] Due to the lack of the red spectral component, the usage of these WLEDs is often limited in industrial and commercial fields. To overcome these limitations, an additional complementary blue light excitable red-emitting phosphor is essential to improve the CRI value (>85) for obtaining the warm or natural white light. In general, Eu^{2+} ions activated metal oxide phosphors show broad emission bands in the blue, green or red spectral region under ultraviolet (UV) or visible wavelength excitations. Enormous research efforts have been extensively devoted to improve the broadband red emission by Eu^{2+} ions activated sulfide- and nitride-based phosphors such as $BaLa_2Si_2S_8:Eu^{2+}$,[14] (Ca, Sr)S:Eu^{2+},[15] $CaAlSiN_3:Eu^{2+}$,[16] $Sr_2Si_5N_8:Eu^{2+}$,[17] and $SrAlSi_4N_7:Eu^{2+}$ (ref. 18) due to the dipole-allowed 4f → 5d electronic transitions. Nevertheless, these sulfide-based phosphors are thermally unstable and moisture-sensible.[19,20] On the other hand, the synthesis of nitride-based phosphors often requires high temperature, high pressure, and vigorous inert gas conditions.[7,12,21] Consequently, it is important to investigate the novel broadband red-emitting phosphors with an excitation band in the blue spectral region.

Garnet-type structures having the general formula of $A_3B_2X_3O_{12}$ (A = Ca, Sr, B = Y, Ga, In, Sc, Al and X = Si, Ge) have been receiving much attention in crystal chemistry owing to their good structural, physical, chemical, and thermal

Department of Electronic Engineering, Institute for Wearable Convergence Electronics, Kyung Hee University, Yongin-si, Gyeonggi-do 446-701, Republic of Korea. E-mail: jsyu@khu.ac.kr; Fax: +82-31-206-2820; Tel: +82-31-201-3820

properties.[2,22–24] In the compound formula, A, B, and X atoms are located in dodecahedral, octahedral, and tetrahedral sites and are surrounded by 8, 6, and 4 oxygen atoms to make a polyhedron.[24,25] The rare-earth (RE) ions activated garnet-type silicate phosphors in a long run have been proved as effective host materials for luminescent properties. Currently, germanate garnet-type phosphors, such as $Ca_3Ga_2Ge_3O_{12}$:Cr^{3+}/Bi^{3+},[26] $Mg_3Y_2Ge_3O_{12}$:Ce^{3+},[27] and $Ca_3Ln_2Ge_3O_{12}$:Eu^{3+} (Ln = Pr^{3+}, Nd^{3+}, Sm^{3+}, Gd^{3+}, Dy^{3+}), have also been studied.[28] This is because the Si and Ge belong to the same fourth elemental group and have the same outer electronic distribution in the periodic table. As per going through the literature, until now, there exist no other reports on Eu^{2+} ions activated broadband red-emitting $Sr_3Y_2Ge_3O_{12}$ phosphors. Thus, we selected the $Sr_3Y_2Ge_3O_{12}$ as a host material which belongs to the garnet family and possesses the cubic structure with a space group $1a\bar{3}d$ (230).

Classically, RE ions activated metal oxide phosphors have been prepared by a conventional solid-state reaction method. This method needs high temperature over a long time and shows micrometer-sized particles with many impurities during the mechanical grinding process, which results in the lower luminescence intensity. However, to solve these problems and reduce the particle size, several finest wet-chemical methods such as hydrothermal,[29] solvothermal,[30] combustion,[31] spray pyrolysis,[32] sol–gel,[33] co-precipitation,[34] and pechini-type sol–gel[35] were employed. Among them, the pechini-type sol–gel method is one of the best attractive and useful methods for the preparation of phosphor materials with definite morphology and is favorable to enhance the luminescent intensity. Pechini synthesis process consists of stable metal complex formation *via* the citric acid or salicylic acid and further proceeds the polyesterification with organic polymerizing agents such as ethylene glycol or polyethylene glycol, forming polymeric resins. The metal complexes can be tied up with the rigid polymeric network and decrease the segregation in between the metal ions, which assures the compositional homogeneity of all the reactants. Therefore, in this work, we reported the synthesis of $Sr_3Y_2Ge_3O_{12}$ phosphor samples with different Eu^{2+} ion concentrations by the pechini-type sol–gel method. The structural and morphological properties were examined by X-ray diffraction (XRD) patterns and field-emission transmission electron microscope (FE-TEM) images, respectively. A systematic study on the photoluminescence (PL) properties of $Sr_3Y_2Ge_3O_{12}$:Eu^{2+} phosphors was carried out in detail. Additionally, a WLED was implemented using a blue LED chip coated with the blend of the commercial YAG:Ce^{3+} phosphor and the $Sr_3Y_2Ge_3O_{12}$:Eu^{2+} red-emitting phosphor. It is found that the fabricated WLED exhibits higher CRI value for solid-state lighting and back-lighting applications.

Experimental procedure

A series of $Sr_{3-3x}Eu_{3x}Y_2Ge_3O_{12}$ ($x = 0.005$, to 0.04 mol) phosphor samples were prepared by the pechini-type sol–gel method. The high-purity raw materials (Sigma-Aldrich Co.) such as strontium nitrate ($Sr(NO_3)_2$), yttrium nitrate hexahydrate ($Y(NO_3)_3 \cdot 6H_2O$), germanium oxide (GeO_2), europium nitrate pentahydrate ($Eu(NO_3)_3 \cdot 5H_2O$), citric acid ($HCO(COOH)(CH_2COOH)_2$), and polyethylene glycol (PEG) ($(C_2H_4O)_n \cdot H_2O$) were used according to the stoichiometric ratios. In the typical synthesis process, 3 mol of germanium oxide was mixed with 10 mL of concentrated nitric acid in a small beaker under magnetic stirring and it is diluted with 20 mL of de-ionized (DI) water to attain germanium nitrate solution, labeled as solution I. Secondly, solution II was prepared by adding 2 mol of yttrium nitrate, $3 - 3x$ mol of strontium nitrate, and $3x$ mol of europium nitrate in 180 mL of DI water. The solution I and solution II were stirred separately for 40 min. After that, the solution I was added slowly to the solution II and maintained the stirring for 30 min to attain the homogenous mixture. Later, 16 mol of citric acid (2 : 1 molar ratio of citric acid and total metal ions in the composition) was added as a chelating agent and stirred for 10 min. Finally, 1 g of PEG was prepended as a cross linking agent and the stirring continued for 1 h to get a complete homogeneous solution. Then, the beaker was covered with a polyethylene cap and heated on a hot plate at 85 °C for about 2 h under the stirring. Later on, the polyethylene cap and the magnetic bar were separated from the solution mixture and the solution was left at the same temperature for 8 h. The solution evaporated slowly, producing the homogenous brownish wet gel. After drying the wet gel in an oven at 120 °C for 24 h, a white colored porous solid matrix called as xerogel was formed. The xerogel was ground, heated at 1200 °C for 8 h in the air atmosphere, and again annealed at 1000 °C (rising temperature of 2 °C per min) for 4 h under thermal CO reducing atmosphere. The obtained phosphor samples were employed to assess the further characterization.

Sample characterization

The XRD pattern and Fourier transform infrared (FTIR) spectrum of the $Sr_3Y_2Ge_3O_{12}$:Eu^{2+} (hereafter referred as SYGO:Eu^{2+}) phosphor samples were recorded on a Mac Science M18XHF-SRA X-ray powder diffractometer and a Thermo Nicolet-5700 FTIR spectrophotometer with the KBr pellet method, respectively. The morphological properties were measured by using a FE-TEM (JEOL JEM-2100F). The PL spectra were studied by using a fluorescence spectrometer (FluoroMate FS-2, Scinco, South Korea) and the lifetime was evaluated on a Photon Technology International (PTI, USA) phosphorimeter with a Xe flash lamp of 25 W power. Thermal PL properties were recorded on the fluorescence spectrometer (FluoroMate FS-2, Scinco, South Korea) equipped with a thermocouple in the temperature range of 30–210 °C (NOVA ST540). In addition, the quantum yield measurement was performed by using a Hamamatsu Photonics C9920-02 system with an integrating sphere.

Results and discussion

XRD, FE-TEM and FTIR analyses of SYGO:0.01Eu^{2+} phosphor

Fig. 1(a) shows the XRD patterns of the SYGO host lattice, SYGO:0.01Eu^{3+} phosphor and SYGO:0.01Eu^{2+} phosphor after annealing in air and thermal CO reducing atmosphere,

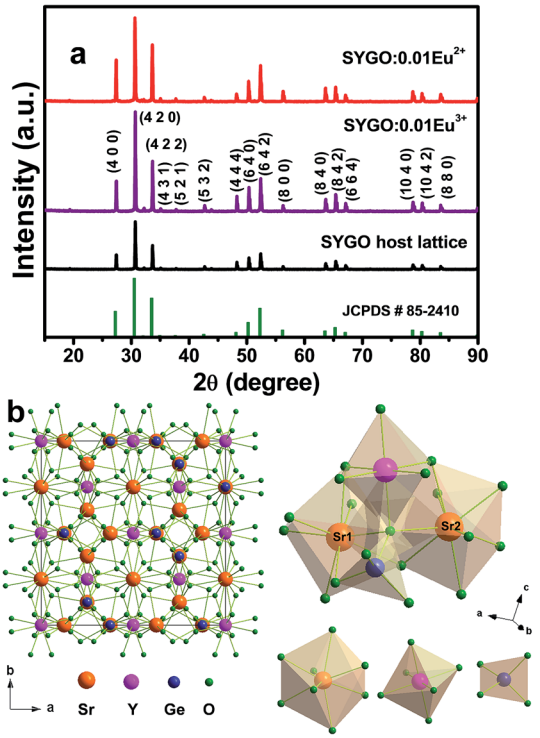

Fig. 1 (a) XRD patterns of the SYGO host lattice, SYGO:0.01Eu^{3+} phosphor, and SYGO:0.01Eu^{2+} phosphor after annealing in air at 1200 °C and thermal CO reducing atmosphere at 1000 °C, respectively and (b) crystal structure drawn using the Diamond software.

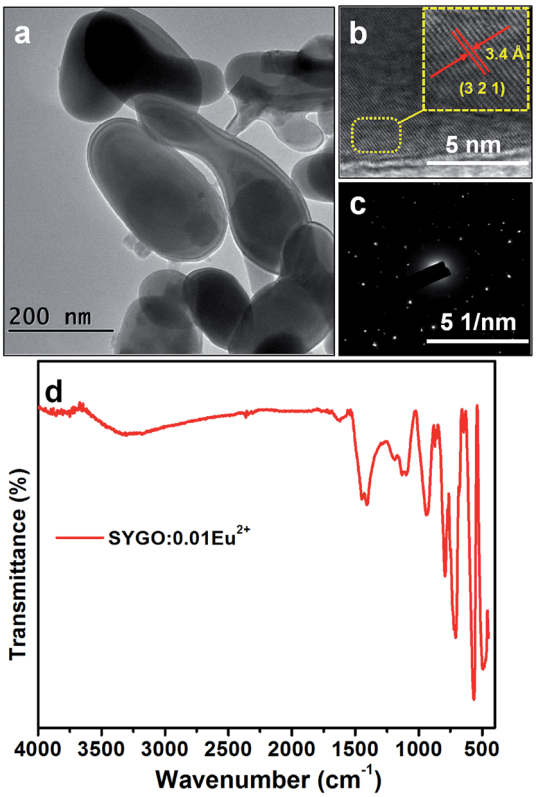

Fig. 2 (a) FE-TEM image, (b) HRTEM image, (c) SAED pattern, and (d) FTIR spectrum of the SYGO:0.01Eu^{2+} phosphor.

respectively. It can be observed that all the diffraction peaks of the three phosphor samples were well consistent with the available standard JCPDS # 85-2410 card. This is attributed to the pure cubic crystal phase of garnet with a space group $la\bar{3}d$ (230). The pure phase form indicates that the Eu^{2+} ions are completely dissolved into the Sr^{2+} sites of the SYGO host lattice and did not exhibit any new significant phase in the present synthesis process. The full width at half maximum (FWHM) of the strongest XRD peak is utilized to determine the crystallite/grain sizes of the SYGO:0.01Eu^{2+} phosphor by the well-known Scherrer formula of $D_{hkl} = k\lambda/\beta \cos\theta$, where D is the average crystallite size, k (0.9) is a shape factor, λ is the X-ray wavelength which is 1.5406 Å, β is the FWHM, and θ is the corresponding Bragg's diffraction angle of the observed peaks. Thus, the calculated average crystallite size of the SYGO:0.01Eu^{2+} phosphor is 97 nm. According to the data in the JCPDS # 85-2410 card, the SYGO garnet crystal structure belongs to the cubic system with a space group $la\bar{3}d$ (230), showing the body-centered cubic symmetry in a unit cell lattice. The SYGO garnet is iso-structural to the $Ca_3Y_2Ge_3O_{12}$ garnet phase and the ideal unit cell crystal structure was drawn using a Diamond software as shown in Fig. 1(b). From the crystal structure, the Sr^{2+}, Y^{3+}, and Ge^{4+} ions were surrounded by 8, 6, and 4 oxygen anions, leading to the dodecahedron, octahedron, and tetrahedron, respectively. On account of the ionic radii or valence state, the Eu^{2+} ions are expected to occupy the Sr^{2+} sites in the SYGO crystal structure.

Fig. 2(a) shows the FE-TEM image of the SYGO:0.01Eu^{2+} phosphor after annealing under the CO reducing atmosphere. The FE-TEM image revealed the inhomogeneous spherical-shaped morphology with non-identical particle sizes. The spherical-shaped morphology would be favorable to produce more stable efficient white light for solid-state lighting applications.[36,37] It is observed that the particle size (>200 nm) is different from the calculated crystallite/grain size from the XRD (97 nm) because a particle may be composed of one or more crystallites.[38] Fig. 2(b) and (c) represents the high-resolution TEM (HRTEM) image and the corresponding selected area electron diffraction (SAED) pattern of the single particle of SYGO:0.01Eu^{2+} phosphor. The HRTEM image showed a d-spacing of 3.4 Å, corresponding to the (321) plane of the phosphor sample, and it well coincided with the cubic phase of the garnet in the XRD. From the SAED pattern, it is clear that the diffraction spots were in doted pattern which confirms the single crystalline nature of the SYGO:0.01Eu^{2+} phosphor. Fig. 2(d) shows the FTIR spectrum of the as-synthesized SYGO:0.01Eu^{2+} phosphor sample. This spectrum exhibited absorption peaks at 3306 and 1616 cm^{-1} which can be attributed to the stretching and bending vibrations of the O–H bonds due to absorption of water on the surface of the phosphor sample.[38,39] The sharp band at 1405 cm^{-1} can be attributed to the bending mode of O–H bonds.[40,41] It can be also observed that strong absorption bands at 934, 792, and 711 cm^{-1} are related to the asymmetric vibration of Ge–O bonds.[42] The sharp

peaks at 562 and 482 cm^{-1} represent the characteristic vibration modes of Ge–O–Ge bonds.[40,42]

PL properties and quantum yield of SYGO:Eu^{2+} phosphors

Fig. 3 shows the PL excitation (PLE) and PL emission spectra of the SYGO:0.01Eu^{2+} phosphor sample. The PLE spectrum consists of two broad bands which cover the wavelength from UV to visible regions (200 to 600 nm) when it was monitored at 612 nm emission wavelength. The first broadband ranging from 220 to 320 nm occurred with the band maxima at 270 nm due to the electronic transition between the valance and conduction bands of the host lattice. Another broadband was located in the wavelength range of 375 to 600 nm with the band maxima at 468 nm and it also consists of several sub-bands centered at 440, 452, 484, and 493 nm which is ascribed to the $4f^7 \rightarrow 4f^65d^1$ electronic transition of Eu^{2+} ions. Under 468 nm blue excitation, the PL emission of the SYGO:0.01Eu^{2+} phosphor exhibited a single and symmetric broad red emission band localized between 540 to 750 nm with the band maxima at 612 nm corresponding to the $4f^65d^1 \rightarrow 4f^7$ transition of Eu^{2+} ions. The broad red emission band also consisted of Eu^{3+} emission peak in the region of 650 to 670 nm with the band maxima at 660 nm due to the $^5D_0 \rightarrow {}^7F_3$ electronic transition. Under 270 nm excitation, a similar red emission band occurred significantly with lower intensity. The broad red emission band of the SYGO:0.01Eu^{2+} phosphor showed higher emission intensity at 468 nm excitation wavelength with a FWHM value of 80 nm. Consequently, the prepared SYGO:0.01Eu^{2+} phosphor revealed broadband red emission under UV and visible wavelength excitations.

In order to find an optimum concentration, a series of SYGO:Eu^{2+} phosphor samples with different concentrations of Eu^{2+} ions were prepared. The PL emission spectra taken at an excitation wavelength of 468 nm are shown in Fig. 4(a). The broadband red emission intensity was increased with increasing the Eu^{2+} ion concentration up to 0.01 mol. The emission intensity decreased with further increasing the Eu^{2+} ion concentration (0.02, 0.03 and 0.04 mol) due to the concentration quenching phenomena and it is ascribed to the non-radiative energy transfer between the adjacent Eu^{2+} ions. The non-radiative energy process exists due to the radiation reabsorption, electric multipolar interactions or exchange interactions. It is obvious that the energy transfer between the Eu^{2+} ions of SYGO phosphors should not be dominated by the exchange interaction due to the allowed $4f^7 \rightarrow 4f^65d^1$ electronic transition. The radiative reabsorption occurs due to the spectral overlap of PLE and PL emission spectra, which is not fully accountable for non-radiative energy transfer between the Eu^{2+} ions in the present study. Thus, the energy transfer between the Eu^{2+} ions should be controlled by electric multipolar interactions. Based on Dexter theory,[43,44] the concentration quenching mechanism of interaction between the two adjacent Eu^{2+} ions is calculated by the following expression:

$$\log\left(\frac{I}{C}\right) = K - \left(\frac{\theta}{3}\right)\log(C). \quad (1)$$

Here, I and K are the luminescence intensity and activator constant, C is the optimum substituted mole fraction of the Eu^{2+} ions (0.01 mol) and θ is the electric multipolar parameter. The θ = 3, 6, 8, and 10 correspond to the exchange coupling, dipole–dipole, dipole–quadrupole, and quadrupole–quadrupole interactions, respectively. Fig. 4(b) shows the linear

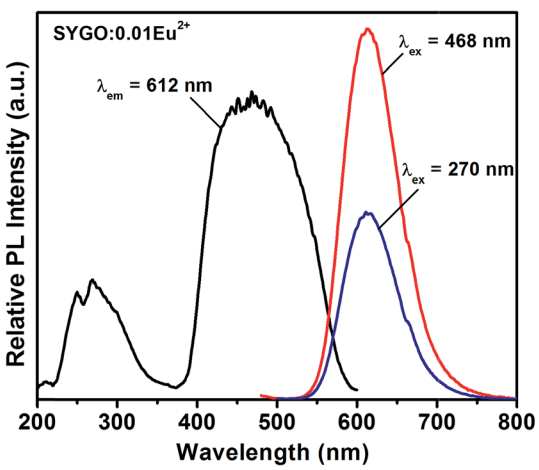

Fig. 3 PLE (λ_{em} = 612 nm) and PL emission (λ_{ex} = 270 and 468 nm) spectra of the SYGO:0.01Eu^{2+} phosphor.

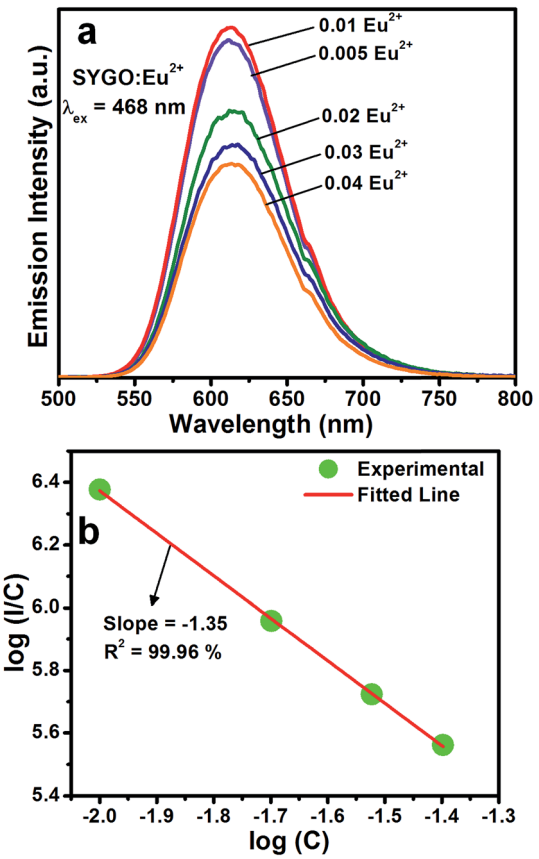

Fig. 4 (a) PL emission spectra of SYGO:Eu^{2+} phosphors as a function of Eu^{2+} ion concentration at 468 nm excitation wavelength. (b) Relationship of log(*C*) *versus* log(*I*/*C*) for SYGO:Eu^{2+} phosphors.

relationship between the $\log(C)$ *versus* $\log(I/C)$ of Eu^{2+} ions. This curve was well fitted by a straight line with a slope of −1.35. The calculated value of θ is 9.6, which is close to 10. Therefore, the quadrupole–quadrupole interactions are responsible for non-radiative energy transfer mechanism between the Eu^{2+} ions.

To estimate the lifetime of the optimized SYGO:0.01Eu^{2+} phosphor sample, the luminescence decay curve was measured under 612 nm emission and 468 nm excitation wavelengths as shown in Fig. 5(a). The decay profile was well fitted to a second-order exponential function as follows:[45]

$$I(t) = I_0 + A_1 \exp\left(\frac{-t}{\tau_1}\right) + A_2 \exp\left(\frac{-t}{\tau_2}\right), \quad (2)$$

where I_0 and $I(t)$ are the luminescence intensities at initial time $t = 0$ and time t, respectively. A_1 and A_2 are constants and τ_1 and τ_2 are the slow decay times for exponential functions. Thus, the average lifetime can be determined by the following expression:

$$\tau_{avg} = \frac{A_1\tau_1^2 + A_2\tau_2^2}{A_1\tau_1 + A_2\tau_2}. \quad (3)$$

Accordingly, the average lifetime value was found to be around 28 μs. The double exponential curve fitting is due to the existence of the two Sr luminescent centers as explored in the SYGO crystal structure. The quantum efficiency (η) was measured by the integrated sphere method for the optimized SYGO:0.01Eu^{2+} phosphor sample. Under the present synthesis condition, the obtained η value for the SYGO:0.01Eu^{2+} phosphor sample at 612 nm emission and 468 nm excitation wavelengths was ~28.3%. The Commission International de l'eclairage (CIE) chromaticity coordinate values were calculated by taking the emission wavelength range from 500 to 800 nm of the SYGO:0.01Eu^{2+} phosphor as shown in Fig. 5(b). The obtained CIE values (0.6146, 0.3837) were found in the reddish-orange region and the matching luminescent photograph of the phosphor is shown in the inset of Fig. 5(b).

Thermal stability and warm WLED fabrication process of SYGO:0.01Eu^{2+} phosphor

Thermal stability is one of the scientific properties of the synthesized phosphor materials due to their considerable impact on the light output, chromaticity, and CRI in practical applications of high-power WLEDs. Fig. 6(a) represents the temperature-dependent PL emission spectra of the SYGO:0.01Eu^{2+} phosphor sample excited at 468 nm in the temperature range of 30 to 210 °C at an interval of 20 °C. From the PL emission spectra, it is clear that the PL emission

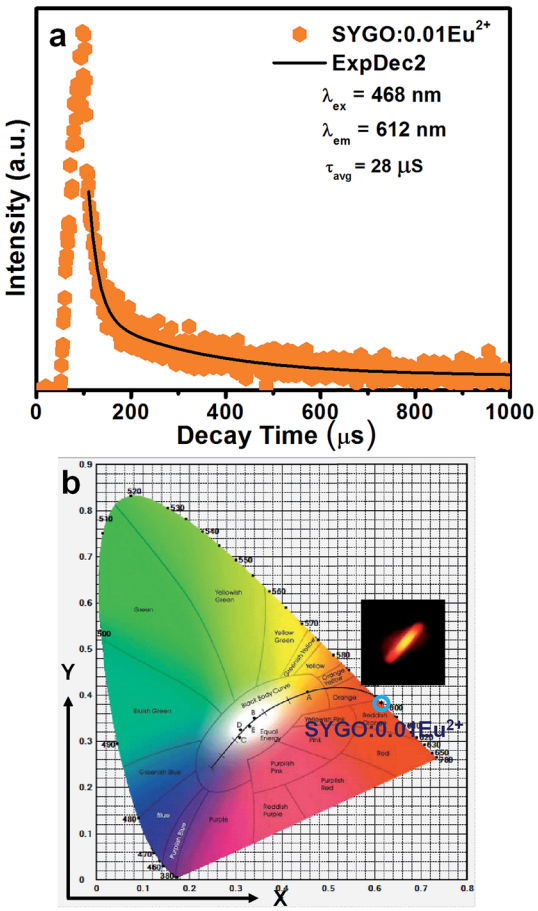

Fig. 5 (a) Decay curve and (b) CIE chromaticity diagram with the corresponding luminescent photograph of the optimized SYGO:0.01Eu^{2+} phosphor sample.

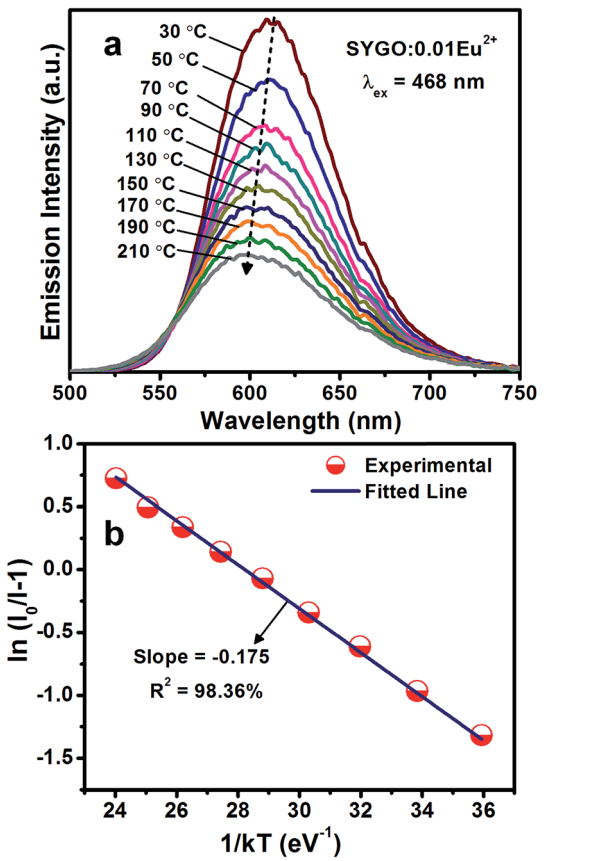

Fig. 6 (a) Temperature-dependent PL emission spectra of the SYGO:0.01Eu^{2+} phosphor at 468 nm excitation wavelength and (b) the corresponding plot of $\ln(I_0/I - 1)$ *versus* $1/kT$.

intensity of the SYGO:0.01Eu^{2+} phosphor gradually decreased with increasing the temperature. The PL emission intensity of the sample was maintained to approximately 52% at 130 °C with respect to the initial intensity at 30 °C. The loss of the reaming 48% emission intensity is due to the thermal quenching phenomena in the SYGO:0.01Eu^{2+} phosphor. In this manner, the impressive thermal stability of the phosphor strongly gives aid to the high-power WLED applications. The thermal quenching behavior occurs due to the non-radiative transition from the 4f^{6}5d^1 excited state to the 4f^7 ground state of Eu^{2+} ions.[46] Furthermore, the red emission spectrum of the SYGO:0.01Eu^{2+} phosphor was blue-shifted above 15 nm with increasing the temperature as shown in Fig. 6(a). The obtained blue-shift is due to the thermally active phonon-assisted excitation from a lower energy emission band to a high-energy emission band of Eu^{2+} ions in the configuration coordinate diagram.[46,47] The activation energy (E_a) for the thermal quenching of the SYGO:0.01Eu^{2+} phosphor was calculated by the following Arrhenius equation:[48,49]

$$\ln\left(\frac{I_0}{I}\right) = \ln A - \frac{E_a}{kT}, \quad (4)$$

where I_0 and I are the emission intensities of the phosphor at room temperature and applied temperature, respectively. A is an Arrhenius constant, T is the temperature, and k is a Boltzmann's constant (8.617×10^{-5} eV K^{-1}). Fig. 6(b) shows the plots of $\ln(I_0/I - 1)$ *versus* $1/kT$. The experimental data were well fitted by a linear fit with a slope of −0.175, indicating the thermal quenching phenomena accompanied with the Arrhenius activation model. From the Fig. 6(b), the calculated E_a value can be inferred to be 0.175 eV.

Fig. 7 shows the comparative PLE and PL emission spectra of the as-synthesized SYGO:0.01Eu^{2+} red-emitting phosphor with the commercially available YAG:Ce^{3+} phosphor under their corresponding emission and excitation wavelengths, respectively. From the spectra, it is clear that the excitation and emission bands of the SYGO:0.01Eu^{2+} phosphor were strongly overlapped with the emission band of YAG:Ce^{3+} phosphor and, in particular, the excitation peaks at 452 and 468 nm of the both phosphors were well matched with each other. Thus, the prepared red-emitting phosphors with the excitation wavelengths of 445–475 nm strongly serve as the excitation source to compensate the red emission deficiency of the YAG:Ce^{3+}

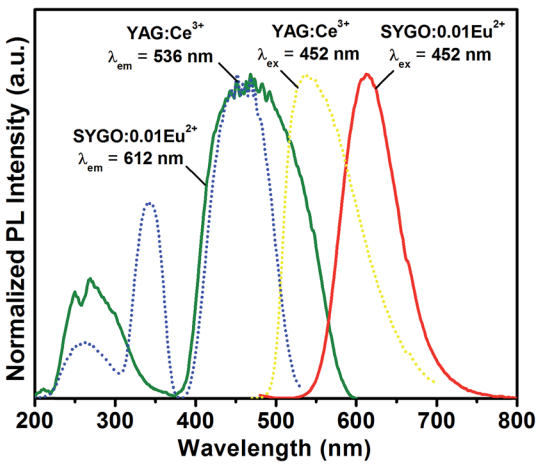

Fig. 7 Comparative PLE and PL emission spectra of the SYGO:0.01Eu^{2+} and commercial YAG:Ce^{3+} phosphors.

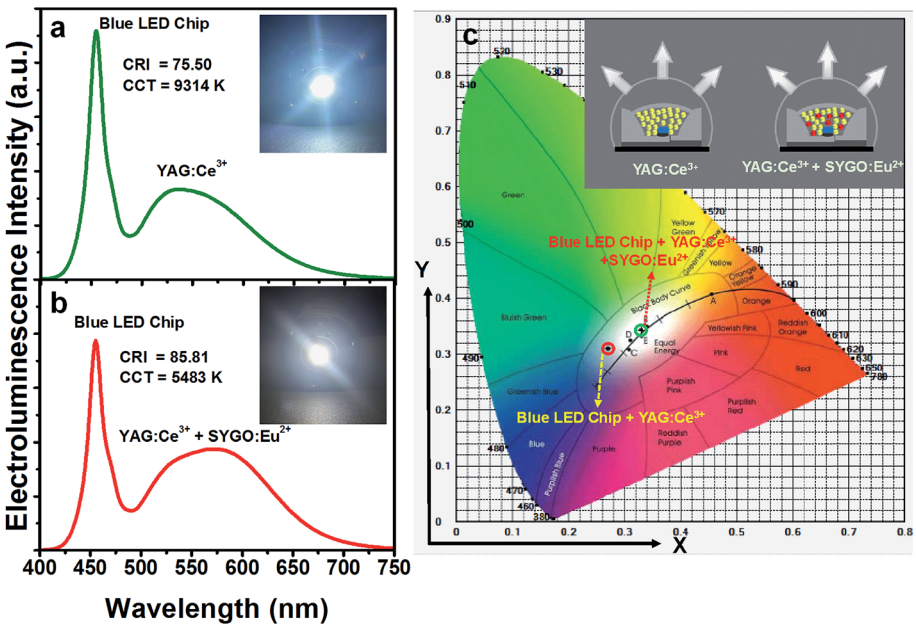

Fig. 8 EL spectra of (a) the commercial YAG:Ce^{3+} phosphor, (b) the mixed YAG:Ce^{3+} and SYGO:0.01Eu^{2+} red-emitting phosphors coated on the 452 nm blue LED chips under a forward-bias current of 30 mA (insets show the corresponding digital photograph images of the packaged WLEDs), and (c) CIE chromaticity coordinates of the YAG:Ce^{3+}- and YAG:Ce^{3+}/SYGO:0.01Eu^{2+}-based WLEDs (inset shows the schematic diagram of the packaged WLEDs).

phosphor and the excitation wavelength region also perfectly matched with the InGaN blue LED excitation. Hence, by mixing the appropriative amounts of the SYGO:0.01Eu^{2+} and YAG:Ce^{3+} phosphors with the blue LED chip, a natural white light was produced for indoor illumination and back-lighting sources.

In order to explore the potentiality of the prepared SYGO:0.01Eu^{2+} phosphor, a WLED package was done by adding this to the YAG:Ce^{3+} phosphor on a 452 nm InGaN blue LED chip. Fig. 8(a) represents the electroluminescence (EL) spectrum of the WLED made with the commercial YAG:Ce^{3+} phosphor under a forward-bias current of 30 mA. The EL spectrum exhibited a broadband emission with the band maxima at about 534 nm due to the corresponding $^2D_{3/2} \rightarrow {}^2F_{5/2}$ and $^2F_{7/2}$ electronic transitions of Ce^{3+} ions. The CRI and CCT values of the fabricated device were 75.5 and 9314 K, respectively. The CIE values were found to be (0.2771, 0.3101). Thus, the fabricated YAG:Ce^{3+}-based WLED emitted a cool white light due to the absence of red-emitting phosphors as shown in the inset of Fig. 8(a). To obtain warm white light, a WLED device was fabricated using the similar 452 nm blue LED chip with a appropriative blend of the YAG:Ce^{3+} phosphor and the SYGO:0.01Eu^{2+} red-emitting phosphor, driven by a 30 mA forward-bias current as shown in Fig. 8(b). The fabricated WLED exhibited the lower CCT (5483 K) and higher CRI (85.81) values compared with the fabricated YAG:Ce^{3+}-based WLED. The obtained CRI and CCT values are excellent prerequisite specifications for illuminating the natural white light. Thus, an obvious emission in the red wavelength region was enhanced by the incorporation of the red-emitting phosphor and the variation in the EL spectrum was clearly observed for the fabricated YAG:Ce^{3+} and YAG:Ce^{3+}/SYGO:0.01Eu^{2+} WLED devices. The inset of Fig. 8(b) shows the warm white-light digital photograph of the fabricated WLED device under the same forward-bias current. It is further noticed that the CIE chromaticity coordinates of the YAG:Ce^{3+}-based WLED in the cool white region (0.2771, 0.3101) were well tuned to the natural white region (0.3300, 0.3439) when mixing the red-emitting phosphor as shown in Fig. 8(c). The inset of Fig. 8(c) represents the schematic diagram of the packaged WLED devices with the InGaN blue LED chips using the YAG:Ce^{3+} phosphor and the mixed YAG:Ce^{3+} and red-emitting phosphors. Consequently, the obtained results demonstrate that the SYGO:0.01Eu^{2+} is a potential red-emitting phosphor to get the warm white light in solid-state lighting and optical display applications.

Conclusions

In summary, we have successfully synthesized the SYGO:Eu^{2+} red-emitting phosphor samples by the pechini-type sol–gel method. The XRD patterns confirmed the cubic phase form of the garnet phosphor with a space group $la\bar{3}d$ (230). The FE-TEM image revealed the spherical-shaped morphology after annealing under the CO reduced atmosphere. The PL emission spectra of the SYGO:Eu^{2+} phosphors showed broad symmetric red band in the wavelength range of 540 to 750 nm with the band maxima at 612 nm due to the allowed $4f^6 5d^1 \rightarrow 4f^7$ electronic transition of Eu^{2+} ions at 468 nm excitation wavelength. The optimum Eu^{2+} ion concentration in SYGO phosphors was found to be 0.01 mol and the quadrupole–quadrupole interactions were involved in the concentration quenching mechanism of Eu^{2+} ions. The temperature-dependent PL emission spectra were explored for the optimized SYGO:0.01Eu^{2+} phosphor, exhibiting good thermal stability with the activation energy of 0.175 eV. The η value of SYGO:0.01Eu^{2+} phosphor at 612 nm emission and 468 nm excitation wavelengths was about 28.3%. Moreover, for the purpose of comparison, the individual commercial YAG:Ce^{3+}-based WLED and the mixed YAG:Ce^{3+} + red-emitting SYGO:0.01Eu^{2+} phosphors-based WLED were fabricated under a forward-bias current of 30 mA. The CRI and CCT values of the YAG:Ce^{3+}/SYGO:0.01Eu^{2+}-based WLED are very much improved and close to a warm white light. Therefore, from all these results, the broadband SYGO:0.01Eu^{2+} red-emitting phosphors are expected to be a promising candidate for the applications of solid-state lighting and back-lighting systems.

Acknowledgements

This work was supported by the National Research Foundation of Korea (NRF) Grant funded by the Korea government (MSIP) (No. 2015R1A5A1037656).

References

1 J. Zhong, W. Zhuang, X. Xing, R. Liu, Y. Li, Y. Liu and Y. Hu, *J. Phys. Chem. C*, 2015, **119**, 5562–5569.
2 Y. F. Wu, Y. H. Chan, Y. T. Nien and I. G. Chen, *J. Am. Ceram. Soc.*, 2013, **96**, 234–240.
3 Z. Xu, Z. Xia, B. Lei and Q. Liu, *J. Mater. Chem. C*, 2016, **4**, 9711–9716.
4 Y. Jin, M.-H. Fang, M. Grinberg, S. Mahlik, T. Lesniewski, M. G. Brik, G.-Y. Luo, J. G. Lin and R.-S. Liu, *ACS Appl. Mater. Interfaces*, 2016, **8**, 11194–11203.
5 H. L. Li, R. J. Xie, N. Hirosaki, T. Takeda and G. H. Zhou, *Int. J. Appl. Ceram. Technol.*, 2009, **6**, 459–464.
6 A. Kitai, *Lumin. Mater. Appl.*, John Wiley & Sons, 2008.
7 D. Deng, H. Yu, Y. Li, Y. Hua, G. Jia, S. Zhao, H. Wang, L. Huang, Y. Li, C. Li and S. Xu, *J. Mater. Chem. C*, 2013, **1**, 3194–3199.
8 W. B. Im, Y.-I. Kim, N. N. Fellows, H. Masui, G. Hirata, S. P. DenBaars and R. Seshadri, *Appl. Phys. Lett.*, 2008, **93**, 1905.
9 Z. Jiang and Y. Wang, *Electrochem. Solid-State Lett.*, 2010, **13**, J68–J70.
10 W.-j. Ding, M. Zhang, R.-j. Yu, J. wang and Q. su, *Acta Sci. Nat. Univ. Sunyatseni*, 2008, **4**, 014.
11 X. Ding, Q. Wang and Y. Wang, *Phys. Chem. Chem. Phys.*, 2016, **18**, 8088–8097.
12 J. Ruan, R. J. Xie, N. Hirosaki and T. Takeda, *J. Am. Ceram. Soc.*, 2011, **94**, 536–542.
13 T. Hussain, L. Zhong, M. Danesh, H. Ye, Z. Liang, D. Xiao, C.-W. Qiu, C. Lou, L. Chi and L. Jiang, *Nanoscale*, 2015, **7**, 10350–10356.
14 S.-P. Lee, T.-S. Chan and T.-M. Chen, *ACS Appl. Mater. Interfaces*, 2014, **7**, 40–44.

15 Y. Hu, W. Zhuang, H. Ye, S. Zhang, Y. Fang and X. Huang, *J. Lumin.*, 2005, **111**, 139–145.
16 K. Uheda, N. Hirosaki, Y. Yamamoto, A. Naito, T. Nakajima and H. Yamamoto, *Electrochem. Solid-State Lett.*, 2006, **9**, H22–H25.
17 R.-J. Xie, N. Hirosaki, T. Suehiro, F.-F. Xu and M. Mitomo, *Chem. Mater.*, 2006, **18**, 5578–5583.
18 C. Hecht, F. Stadler, P. Schmidt and W. Schnick, *Z. Anorg. Allg. Chem.*, 2008, **634**, 2044.
19 S. S. Manoharan, S. Goyal, M. L. Rao, M. S. Nair and A. Pradhan, *Mater. Res. Bull.*, 2001, **36**, 1039–1047.
20 B. L. Abrams, W. Roos, P. H. Holloway and H. C. Swart, *Surf. Sci.*, 2000, **451**, 174–181.
21 X. Piao, T. Horikawa, H. Hanzawa and K.-i. Machida, *Appl. Phys. Lett.*, 2006, **88**, 161908.
22 O. Lipina, L. Surat, M. Melkozerova, A. Tyutyunnik, I. Leonidov and V. Zubkov, *Opt. Spectrosc.*, 2014, **116**, 695–699.
23 Y. Liu, J. Hao, W. Zhuang and Y. Hu, *J. Phys. D: Appl. Phys.*, 2009, **42**, 245102.
24 D. Chen, Y. Chen, H. Lu and Z. Ji, *Inorg. Chem.*, 2014, **53**, 8638–8645.
25 D. Pasiński, E. Zych and J. Sokolnicki, *J. Alloys Compd.*, 2015, **653**, 636–642.
26 C. Liu, Z. Xia, M. S. Molokeev and Q. Liu, *J. Am. Ceram. Soc.*, 2015, **98**, 1870–1876.
27 Z. Jiang, Y. Wang and L. Wang, *J. Electrochem. Soc.*, 2010, **157**, J155–J158.
28 F. Piccinelli, A. Lausi and M. Bettinelli, *J. Solid State Chem.*, 2013, **205**, 190–196.
29 B. Yan and J.-H. Wu, *Mater. Chem. Phys.*, 2009, **116**, 67–71.
30 X. Li, H. Liu, J. Wang, H. Cui, S. Yang and I. Boughton, *J. Phys. Chem. Solids*, 2005, **66**, 201–205.
31 T. Peng, H. Yang, X. Pu, B. Hu, Z. Jiang and C. Yan, *Mater. Lett.*, 2004, **58**, 352–356.
32 Y. Shimomura and N. Kijima, *J. Electrochem. Soc.*, 2004, **151**, H192–H197.
33 I.-C. Chen and T.-M. Chen, *J. Mater. Res.*, 2001, **16**, 644–651.
34 J. H. Zeng, J. Su, Z. H. Li, R. X. Yan and Y. D. Li, *Adv. Mater.*, 2005, **17**, 2119–2123.
35 M. Pang, X. Liu and J. Lin, *J. Mater. Res.*, 2005, **20**, 2676–2681.
36 G. S. R. Raju, H. C. Jung, J. Y. Park, C. Kanamadi, B. K. Moon, J. H. Jeong, S.-M. Son and J. H. Kim, *J. Alloys Compd.*, 2009, **481**, 730–734.
37 D. Geng, G. Li, M. Shang, C. Peng, Y. Zhang, Z. Cheng and J. Lin, *Dalton Trans.*, 2012, **41**, 3078–3086.
38 S. K. Hussain and J. S. Yu, *J. Lumin.*, 2016, **175**, 100–105.
39 M. Runowski, T. Grzyb, A. Zep, P. Krzyczkowska, E. Gorecka, M. Giersig and S. Lis, *RSC Adv.*, 2014, **4**, 46305–46312.
40 Y. Cao, G. Zhu and Y. Wang, *RSC Adv.*, 2015, **5**, 65710–65718.
41 L. K. Bharat and J. S. Yu, *J. Nanosci. Nanotechnol.*, 2013, **13**, 8239–8244.
42 V. Zubkov, I. Leonidov, A. Tyutyunnik, N. Tarakina, I. Baklanova, L. Perelyaeva and L. Surat, *Phys. Solid State*, 2008, **50**, 1699–1706.
43 D. L. Dexter, *J. Chem. Phys.*, 1953, **21**, 836–850.
44 B. Wang, H. Lin, J. Xu, H. Chen and Y. Wang, *ACS Appl. Mater. Interfaces*, 2014, **6**, 22905–22913.
45 M. P. Saradhi and U. Varadaraju, *Chem. Mater.*, 2006, **18**, 5267–5272.
46 L. Chen, C.-C. Lin, C.-W. Yeh and R.-S. Liu, *Materials*, 2010, **3**, 2172–2195.
47 C. C. Lin and R.-S. Liu, *J. Phys. Chem. Lett.*, 2011, **2**, 1268–1277.
48 N. Zhang, C. Guo, J. Zheng, X. Su and J. Zhao, *J. Mater. Chem. C*, 2014, **2**, 3988–3994.
49 J. Chen, N. Zhang, C. Guo, F. Pan, X. Zhou, H. Suo, X. Zhao and E. M. Goldys, *ACS Appl. Mater. Interfaces*, 2016, **8**, 20856–20864.

